Boron Clusters

International Edition: DOI: 10.1002/anie.201902406
German Edition: DOI: 10.1002/ange.201902406

High-Resolution Photoelectron Imaging of IrB_3^-: Observation of a π-Aromatic B_3^+ Ring Coordinated to a Transition Metal

Joseph Czekner, Ling Fung Cheung, G. Stephen Kocheril, Maksim Kulichenko, Alexander I. Boldyrev, and Lai-Sheng Wang**

Abstract: *In a high-resolution photoelectron imaging and theoretical study of the IrB_3^- cluster, two isomers were observed experimentally with electron affinities (EAs) of 1.3147(8) and 1.937(4) eV. Quantum calculations revealed two nearly degenerate isomers competing for the global minimum, both with a B_3 ring coordinated with the Ir atom. The isomer with the higher EA consists of a B_3 ring with a bridge-bonded Ir atom (C_s, $^2A'$), and the second isomer features a tetrahedral structure (C_{3v}, $^2A_1$). The neutral tetrahedral structure was predicted to be considerably more stable than all other isomers. Chemical bonding analysis showed that the neutral C_{3v} isomer involves significant covalent Ir–B bonding and weak ionic bonding with charge transfer from B_3 to Ir, and can be viewed as an Ir–(η^3-B_3^+) complex. This study provides the first example of a boron-to-metal charge-transfer complex and evidence of a π-aromatic B_3^+ ring coordinated to a transition metal.*

The electron deficiency of boron leads to unique delocalized bonds in boron compounds and clusters, which can exhibit π and σ double aromaticity. A review specifically focused on the double aromaticity of three-centered boron rings appeared in 2006.[1] The B_3^- anionic cluster is the smallest possible doubly (π and σ) aromatic system.[2] The B_3^+ cation is only π-aromatic and has recently been observed in complexes with CO and N_2.[3] A previous computational study suggested that B_3^- might be stabilized by Na^+ to form an $Na^+B_3^-$ salt.[4] Two alkali-stabilized boron clusters were observed previously, LiB_6^- and LiB_8^-.[5] Both species had similar structures to their analogous pure boron cluster dianions, suggesting that it is possible to stabilize aromatic boron clusters with alkali metals. A theoretical study has examined the stability of the B_3^- ring in sandwich complexes with alkali and alkali earth elements.[6] It was found that only heterodecked sandwiches were stable when capped with cyclopentadienyl (Cp^-). Recently, a π-aromatic B_3 ring was synthesized as $B_3R_3^{2-}$ stabilized by Na^+ and sterically protected by bulky ligands.[7] The bonding in $B_3R_3^{2-}$ was found to be identical to that in $B_3H_3^{2-}$, which is analogous to $C_3H_3^+$.[8] Doubly aromatic three-membered-ring bishomotriboriranide and triboracyclopropanate were also synthesized as lithium salts.[9] Boranes with as few as three or four boron atoms are known,[10] including several metalloboranes with iridium,[10i] although their bonding is quite different from the bare boron clusters.[2]

Anion photoelectron spectroscopy (PES) has been shown to be a powerful technique to probe the electronic structure and chemical bonding of size-selected boron clusters.[11] Combined with theoretical calculations, PES has also been used to elucidate numerous transition-metal-doped boron clusters.[12] In particular, the PE spectrum of TaB_3^- revealed that the Ta–B interactions are stronger than B–B interactions because its lowest-energy structure features a Ta atom inserted into a B–B bond of the B_3 ring.[12n] On the other hand, the lowest-energy structure of AuB_3^- contained a B_3 ring with the Au atom bonded to an apex B atom,[12j] revealing a very different Au–B bonding mode that is analogous to the H–B bond.[13] Joint PES and theoretical studies of lanthanide-doped boron clusters have been reported recently, revealing both half-sandwich[14] and inverse-sandwich complexes,[15] as well as several transition-metal diboride clusters.[16] Most recently, a small lanthanide-doped boron cluster, PrB_3^-, was found to be planar with $Pr^{II}[\eta^2\text{-}B_3^{3-}]$ coordination.[17] The question we were trying to address in this study is whether three-membered aromatic boron rings can coordinate with a transition metal in η^3-B_3 coordination while retaining σ or π aromaticity.

Herein we report a high-resolution PE imaging (PEI) and theoretical study of the IrB_3^- cluster. Two isomers were observed in the PEI experiment. Theoretical calculations found two nearly degenerate low-lying isomers: a quasiplanar isomer with an η^2-B_3 moiety coordinated to Ir, and a tetrahedral structure with an η^3-B_3 moiety coordinated to Ir. In the neutral potential-energy surface, the tetrahedral structure was found to be much more stable than all other isomers owing to favorable Ir–B covalent bonding and weak electron donation from the B_3 ring to Ir to form a $(B_3)^+Ir^-$ cluster with a π-aromatic B_3^+ moiety. This compound is the first example of a transition-metal-doped boron cluster in which the negative charge is donated from the boron ring to a metal center.

The PEI experiment was performed on a high-resolution photoelectron imaging apparatus.[18,19] Figure 1 shows the reconstructed PE images and spectra measured at photon energies of 2.3305 and 3.4958 eV. The PE spectrum taken at 2.3305 eV (Figure 1a) reveals two bands (X' and X), each with well-resolved vibrational progressions around 1.3 and 2.0 eV. By varying the cluster temperature,[11] we found that

[*] J. Czekner, L. F. Cheung, G. S. Kocheril, Prof. L.-S. Wang
Department of Chemistry, Brown University
324 Brook Street, Providence, Rhode Island 02912 (USA)
E-mail: lai-sheng_wang@brown.edu
M. Kulichenko, Prof. A. I. Boldyrev
Department of Chemistry and Biochemistry, Utah State University
0300 Old Main Hill, Logan, Utah, 84322 (USA)
E-mail: a.i.boldyrev@usu.edu
Supporting information and the ORCID identification number(s) for the author(s) of this article can be found under: https://doi.org/10.1002/anie.201902406.

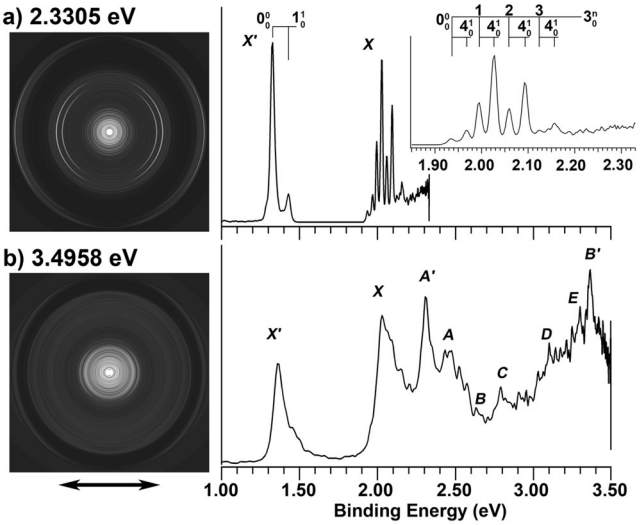

Figure 1. Photoelectron images and spectra at a) 2.3305 eV (532.00 nm) and b) 3.4958 eV (354.67 nm). The vertical lines denote vibrational progressions. The insert in (a) shows the vibrational assignments for band *X*. The double arrow below the images shows the laser polarization.

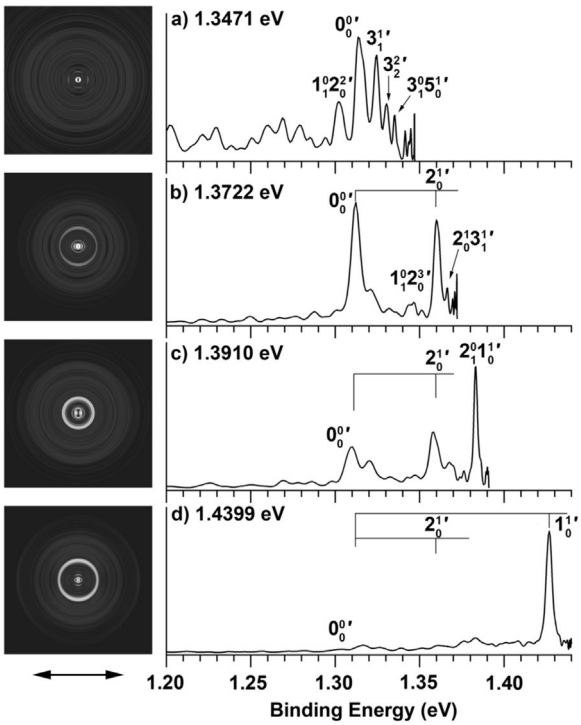

Figure 2. High-resolution photoelectron images and spectra at a) 1.3471 eV (920.38 nm), b) 1.3722 eV (903.54 nm), c) 1.3910 eV (891.33 nm), and d) 1.4399 eV (861.06 nm). The vertical lines denote fundamental vibrations; hot band transitions are labeled. The double arrow below the images shows the laser polarization.

these two bands corresponded to two isomers, with band *X′* coming from a slightly higher energy isomer because its relative intensity increased under hotter source conditions (see Figure S1 in the Supporting Information).[19] Band *X′* displays a single vibrational progression with the 0–0 transition centered around 1.32 eV. A second band with its 0–0 peak at 1.937(4) eV exhibits rich vibrational structures. More PES bands were observed in the 3.4958 eV spectrum (*A*–*E*, *A′*, and *B′*). The relative intensities of bands *A′* and *B′* were found to correlate with that of band *X′* (see Figure S1), and they must come from the same isomer. All the observed bands and their binding energies are summarized in Table 1, where they are compared with the theoretical results.

Higher-resolution PE spectra for band *X′* at lower photon energies are presented in Figure 2. The 1.3471 eV spectrum (Figure 2a) shows several well-resolved vibrational features near the 0–0 peak, all coming from hot band transitions. A new intense vibrational peak was observed in the 1.3722 eV spectrum along with two weak hot band transitions (Figure 2b). One more intense peak in Figure 2c seems to come from a hot band transition. This peak was identified as a hot band because there are no symmetry-allowed modes close to this frequency (see below). Another intense peak was observed in the 1.4399 eV spectrum (Figure 2d). This peak corresponds to a new vibrational mode (see below). The binding energies and angular distributions of all the observed vibrational transitions are provided in the Supporting Information (see Table S1 and Figures S2–S4).[19]

Table 1: Experimental ADEs and VDEs and the calculated values along with the final neutral states and valence-electron configurations for the two IrB_3^- low-lying isomers.

Isomer A.2/N.2				
Experimental			Theoretical ADE/VDE	
Peak	ADE/VDE	Final state and electronic configuration	TPSS	ROCCSD(T)
X′	1.3147(8)/1.3147(8)	$^1A_1...4a_1^23e^45a_1^24e^46a_1^25e^47a_1^0$	1.34/1.37	1.20/1.28
A′	2.30(5)	$^3E...4a_1^23e^45a_1^24e^46a_1^25e^37a_1^1$	2.53	
B′	3.38(5)	$^1E...4a_1^23e^45a_1^24e^46a_1^25e^37a_1^1$	3.79	
Isomer A.1/N.1				
Experimental			Theoretical ADE/VDE	
Peak	ADE/VDE	Final state and electronic configuration	TPSS	ROCCSD(T)
X	1.937(4)/2.026(4)	$^3B_1...5a_1^26a_1^23b_2^22b_1^27a_1^24b_2^21a_2^28a_1^29a_1^13b_1^1$	1.71/1.85	1.86/2.03
A	2.45(5)	$^1A_1...5a_1^26a_1^23b_2^22b_1^27a_1^24b_2^21a_2^28a_1^29a_1^23b_1^0$	2.45	
B	2.64(5)	$^1B_1...5a_1^26a_1^23b_2^22b_1^27a_1^24b_2^21a_2^28a_1^29a_1^13b_1^1$	2.72	
C	2.80(5)	$^3B_1...5a_1^26a_1^23b_2^22b_1^27a_1^24b_2^21a_2^28a_1^19a_1^23b_1^1$	2.73	
D	3.15(5)	$^3B_2...5a_1^26a_1^23b_2^22b_1^27a_1^24b_2^21a_2^18a_1^29a_1^23b_1^1$	3.31	
E	3.30(5)	$^1B_1...5a_1^26a_1^23b_2^22b_1^27a_1^24b_2^21a_2^28a_1^19a_1^23b_1^1$	3.56	

Theoretical calculations were performed for IrB_3^-.[19] The global minima of IrB_3^- were searched using the coalescence kick method,[20] the TPSS functional,[21] and the lanl2dz basis set.[22] The lowest-energy isomers were reoptimized at the TPSS/aug-cc-pVTZ-PP[23] level of theory. Previous studies on TaB_3^- and B_3Au^- yielded satisfactory results using similar methods.[12m,n] All calculations were performed with the Gaussian 09 program.[24] The three isomers within 0.2 eV of the global minimum are shown in Figure 3 (see Figure S5 for all low-lying isomers within 2 eV of the global

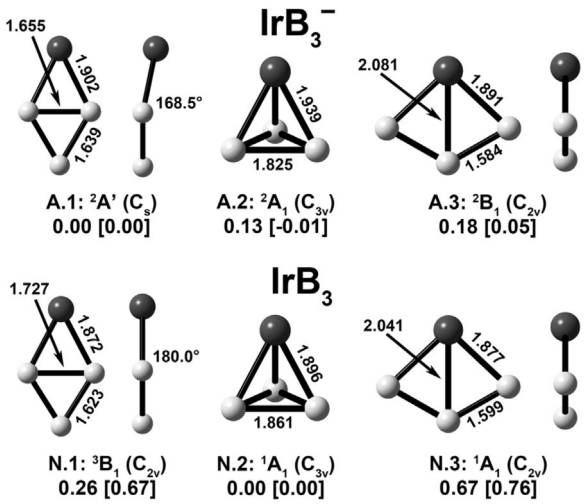

Figure 3. Optimized structures for the ground states and low-lying isomers for IrB_3^- and IrB_3. Bond lengths are given in Å. Relative energies are given in eV at the TPSS level followed by the ROCCSD(T) values in brackets.

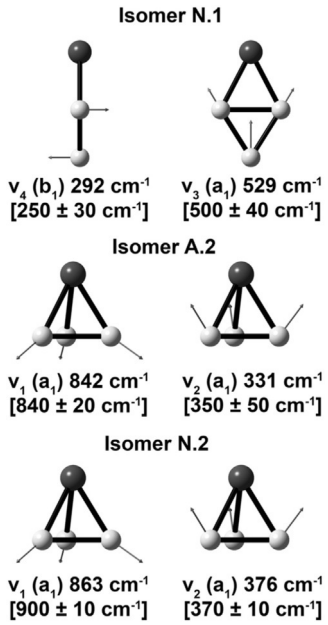

Figure 4. Displacement vectors and computed vibrational frequencies of the observed vibrational modes of isomers A.2, N.1, and N.2 (see Figure 3). The values in brackets are the measured frequencies.

minimum).[19] The lowest-energy anion at the DFT level (isomer A.1) consists of a B_3 ring with a bridge-bonded Ir atom. The second isomer (A.2) has a tetrahedral structure with a B_3 ring capped by the Ir atom. The third isomer (A.3) has a fan structure, which can be viewed as the Ir atom inserted into a B–B bond of a B_3 ring. Using the ROCCSD(T) method, we found that isomers A.1 and A.2 become nearly degenerate with A.2 being 0.01 eV more stable, while isomer A.3 is only slightly higher in energy. The ROCCSD(T) calculations were single-point calculations using the TPSS-optimized geometries, which are not necessarily the minimum on the ROCCSD(T) potential-energy surface. The most stable neutral structures are also shown in Figure 3. The tetrahedral structure with a singlet spin state (N.2) is significantly more stable than the two planar isomers (N.1 and N.3).

The adiabatic (ADE) and vertical detachment energies (VDE) were calculated for each isomer. The ADE for isomers A.2 and A.1 was calculated to be 1.20 and 1.86 eV, respectively, using the ROCCSD(T) method (Table 1). Isomer A.3 was found to have an ADE of 1.90 eV by the same method. Several calculated vibrational frequencies for isomers A.2, N.1, and N.2 are presented in Figure 4 (see Table S2 for the full list of vibrational frequencies).[19]

The calculated ADE for the planar isomer A.1 agrees well with the 0_0^0 transition of band *X* (Table 1). The vibrational peaks in the *X* band are almost evenly spaced, but the alternating intensities of the peaks suggest that two modes are involved, with the frequency of one of the modes almost twice that of the other mode. The geometry changes from A.1 to N.1 (Figure 3) suggest that the two Franck–Condon active modes should be the Ir–B_3 stretching mode ($\nu_3 = 529\ cm^{-1}$) and the bending mode ($\nu_4 = 292\ cm^{-1}$), as shown in Figure 4. There should be a long bending progression off each stretching level. However, the 4_0^2 transitions overlap with the stretching transitions, thus resulting in the uneven vibrational profile. The β values for all of the vibrational peaks are around 0.5 (see Figure S4), thus indicating that the outgoing wave has some *p* character, which is consistent with the predicted detachment from the HOMO orbital that involves the 5d orbital of Ir (see Figure S6). The higher-binding-energy features in Figure 1b can all be assigned using the TDDFT results (Table 1). We can rule out isomer A.3 because none of its calculated vibrational frequencies (see Table S2) match the experimental values.

The 0_0^0 transition of band *X′* agrees well with the calculated ADE for the tetrahedral isomer A.2 (Table 1). The high-resolution spectra in Figure 2 yield accurate vibrational frequencies. Two fundamental progressions for neutral isomer N.2 can be assigned as the Ir–B_3 stretching mode ($(370 \pm 10)\ cm^{-1}$) and B_3 breathing mode ($(900 \pm 10)\ cm^{-1}$), in agreement with the structural changes from A.2 to N.2 (Figure 3). The measured frequencies agree well with the calculated values (Figure 4). Furthermore, we were able to estimate the corresponding vibrational frequencies for the A.2 anion isomer, as compared with the computed values in Figure 4. We can also assign several combination modes (see Table S1) using the calculated frequencies (see Table S2).[19] The 0_0^0 peak of band *X′* has a β value approaching 2 at high kinetic energies owing to the contribution of the $5d_{z^2}$ orbital (see Figure S6), whereas nearly all peaks in Figure 2 have negative β values owing to the interference of the outgoing $p + f$ wave (see Figure S4).[19] Figure 2c,d also shows that the vibrational peaks involving the $1_0^{1'}$ transitions are significantly enhanced, probably as a result of vibronic coupling.

We performed adaptive natural density partitioning (AdNDP) analysis on the neutral species to elucidate the chemical bonding in each isomer (Figure 5).[25] The planar N.1 isomer consists of two 5d lone pairs and four two-center–two-electron (2c-2e) bonds around the periphery from the B 2s and Ir $5d_{yz}$ orbitals (Figure 5b). There are also two 3c-2e

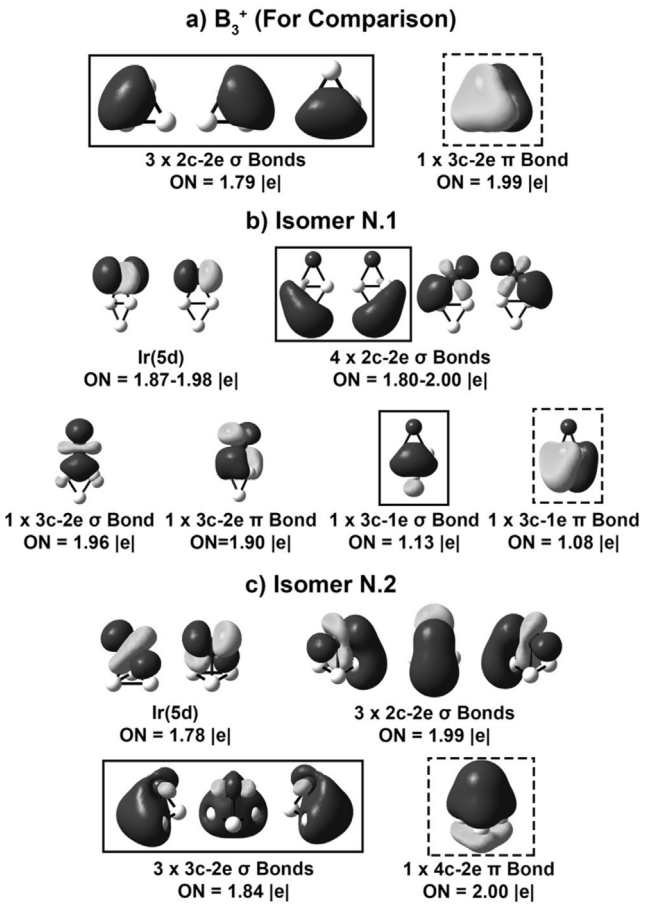

Figure 5. Adaptive natural density partitioning (AdNDP) analysis for isomers N.1 (b) and N.2 (c). The AdNDP result of B_3^+ (a) is given for comparison. The solid and dashed boxes emphasize the σ and π bonds, respectively, in the two isomers of IrB_3 that are similar to those in B_3^+ (a).

bonds involving the B 2p and Ir 5d orbitals, as well as two 3c-1e bonds delocalized over the B_3 ring. The 3c-1e π bond is reminiscent of the 3c-2e bonds in B_3^+ shown in Figure 5a for comparison. The two 3c-1e single-electron bonds are similar to the doubly aromatic σ and π bond in B_3^-;[2] the single-electron bonds are consistent with lower stability of the planar open-shell IrB_3 neutral cluster. It is expected that this isomer would be more competitive in the closed-shell $[IrB_3]^{2-}$ system.

Our AdNDP analysis for the N.2 tetrahedral global minimum (Figure 5c) reveals two 5d lone pairs and three 2c-2e Ir–B bonds. The three 3c-2e bonds mainly describe B–B bonding (see Figure 5a for B_3^+) with contributions also from the $5d_{xy}$ or $5d_{x^2-y^2}$ orbitals, as emphasized in Figure 5c. The 4c-2e bond involves bonding between the Ir 6s orbital and the π bond in B_3^+, thus preserving the π aromaticity in the tetrahedral N.2 isomer. This optimal bonding between Ir and the B_3 ring in the tetrahedral isomer underlies its considerable stability on the neutral potential energy surface. Natural bond orbital (NBO) charge analysis[26] on N.2 gave $Q(\mathrm{Ir}) = -0.394\,e$, which indicates, surprisingly, that charge is transferred from the B_3 unit to the metal. Therefore, isomer N.2 can be viewed approximately as $(B_3)^+Ir^-$, which is the first example of the coordination of a B_3^+ cation to a negatively charged transition metal. The surprising direction of charge transfer can be understood by the high electronegativity of iridium (2.20) as compared to boron (2.04).[27] The ionic interaction provides further stabilization of the tetrahedral isomer. Interestingly, the structures of the MB_3^- clusters depend on the nature of the interactions between M and B. The strong Ta–B bonding results in a fanlike global minimum for TaB_3^-,[12n] whereas the relatively weak Au–B bonding leads to a terminal Au–B bond in AuB_3^-.[12m] The Ir–B bonding is between the Ta–B and Au–B bonding, thus resulting in two nearly degenerate global minima with a side-on Ir–(η^2-B_3) structure and a tetrahedral Ir–(η^3-B_3) structure.

In conclusion, we have reported a high-resolution photoelectron imaging and computational study on the IrB_3^- cluster. Photoelectron spectroscopy revealed the presence of two isomers in the cluster beam of IrB_3^-. Two nearly degenerate low-lying isomers, with a quasiplanar η^2-B_3 moiety coordinated to Ir and an η^3-B_3 tetrahedral structure, were found computationally to compete for the global minimum in the anion. The computed electron binding energies and vibrational frequencies of these two isomers are in good agreement with the experimental results. In the neutral species, tetrahedral IrB_3 was found to be significantly more stable than any other isomers. Chemical bonding analysis revealed strong covalent bonding between Ir and B_3 in the tetrahedral isomer, in which the aromaticity of the B_3 unit is maintained. Surprisingly, it was further found that there is a small amount of charge transfer from the B_3 unit to Ir in the tetrahedral isomer. The current study discloses the smallest π-aromatic system, B_3^+, stabilized by a negatively charged transition metal, which may be viable for bulk synthesis with suitable ligands.

Acknowledgements

Support by the National Science Foundation for the experimental work at Brown University (CHE-1763380 to L.-S.W.) and theoretical work at Utah State University (CHE-1664379 to A.I.B.) is gratefully acknowledged. We also thank both the Center for Computation and Visualization at Brown University and the Centre for High Performance Computing at the University of Utah for computational support and resources.

Conflict of interest

The authors declare no conflict of interest.

Keywords: boron clusters · chemical bonding · computational chemistry · metal–boride clusters · photoelectron spectroscopy

How to cite: *Angew. Chem. Int. Ed.* **2019**, *58*, 8877–8881
Angew. Chem. **2019**, *131*, 8969–8973

[1] M. Hofmann, A. Berndt, *Heteroat. Chem.* **2006**, *17*, 224.
[2] H. J. Zhai, L. S. Wang, A. N. Alexandrova, A. I. Boldyrev, V. G. Zakrzewski, *J. Phys. Chem. A* **2003**, *107*, 9319.

[3] J. Jin, G. Wang, M. Zhou, D. M. Andrada, M. Hermann, G. Frenking, *Angew. Chem. Int. Ed.* **2016**, *55*, 2078; *Angew. Chem.* **2016**, *128*, 2118.
[4] A. E. Kuznetsov, A. I. Boldyrev, *Struct. Chem.* **2001**, *13*, 141.
[5] a) A. N. Alexandrova, H. J. Zhai, L. S. Wang, A. I. Boldyrev, *Inorg. Chem.* **2004**, *43*, 3552; b) A. N. Alexandrova, A. I. Boldyrev, H. J. Zhai, L. S. Wang, *J. Chem. Phys.* **2005**, *122*, 054313.
[6] L. M. Yang, J. Wang, Y. H. Ding, C. C. Sun, *J. Phys. Chem. A* **2007**, *111*, 9122.
[7] T. Kupfer, H. Braunschweig, K. Radacki, *Angew. Chem. Int. Ed.* **2015**, *54*, 15084; *Angew. Chem.* **2015**, *127*, 15299.
[8] A. A. Korkin, P. von R. Schleyer, M. L. McKee, *Inorg. Chem.* **1995**, *34*, 961.
[9] a) M. Unverzagt, G. Subramanian, M. Hofmann, P. von R. Schleyer, S. Berger, K. Harms, W. Massa, A. Berndt, *Angew. Chem. Int. Ed. Engl.* **1997**, *36*, 1469; *Angew. Chem.* **1997**, *109*, 1567; b) C. Präsang, A. Mlodzianowska, Y. Sahin, M. Hofmann, G. Geiseler, W. Massa, A. Berndt, *Angew. Chem. Int. Ed.* **2002**, *41*, 3380; *Angew. Chem.* **2002**, *114*, 3529.
[10] a) Y. Nishihara, K. J. Deck, M. Shang, T. P. Fehlner, *J. Am. Chem. Soc.* **1993**, *115*, 12224; b) Y. Nishihara, K. J. Deck, M. Shang, T. P. Fehlner, B. S. Haggerty, A. L. Rheingold, *Organometallics* **1994**, *13*, 4510; c) S. Aldridge, M. Shang, T. P. Fehlner, *J. Am. Chem. Soc.* **1997**, *119*, 11120; d) D. Y. Kim, Y. You, G. S. Girolami, *J. Organomet. Chem.* **2008**, *693*, 981; e) J. Ho, K. J. Deck, Y. Nishihara, M. Shang, T. P. Fehlner, *J. Am. Chem. Soc.* **1995**, *117*, 10292; f) C. Präsang, M. Hofmann, G. Geiseler, W. Massa, A. Berndt, *Angew. Chem. Int. Ed.* **2002**, *41*, 1526; *Angew. Chem.* **2002**, *114*, 1597; g) W. Mesbah, C. Präsang, M. Hofmann, G. Geiseler, W. Massa, A. Berndt, *Angew. Chem. Int. Ed.* **2003**, *42*, 1717; *Angew. Chem.* **2003**, *115*, 1758; h) B. Le Guennic, H. Jiao, S. Kahlal, J. Y. Saillard, J. F. Halet, S. Ghosh, M. Shang, A. M. Beatty, A. L. Rheingold, T. P. Fehlner, *J. Am. Chem. Soc.* **2004**, *126*, 3203; i) X. Lei, M. Shang, T. P. Fehlner, *Chem. Eur. J.* **2000**, *6*, 2653; j) X. M. Chen, N. N. Ma, Q. F. Zhang, J. Wang, X. G. Feng, C. G. Wei, L. S. Wang, J. Zhang, X. N. Chen, *J. Am. Chem. Soc.* **2018**, *140*, 6718; k) X. M. Chen, N. N. Ma, X. R. Liu, C. G. Wei, C. C. Cui, B. L. Cao, Y. H. Guo, L. S. Wang, Q. F. Gu, X. N. Chen, *Angew. Chem. Int. Ed.* **2019**, *58*, 2720 – 2724; *Angew. Chem.* **2019**, *131*, 2746 – 2750.
[11] L. S. Wang, *Int. Rev. Phys. Chem.* **2016**, *35*, 69.
[12] a) H. J. Zhai, L. S. Wang, D. Y. Zubarev, A. I. Boldyrev, *J. Phys. Chem. A* **2006**, *110*, 908; b) H. J. Zhai, C. Q. Miao, S. D. Li, L. S. Wang, *J. Phys. Chem. A* **2010**, *114*, 12155; c) C. Romanescu, T. R. Galeev, W. L. Li, A. I. Boldyrev, L. S. Wang, *Angew. Chem. Int. Ed.* **2011**, *50*, 9334; *Angew. Chem.* **2011**, *123*, 9506; d) W. L. Li, C. Romanescu, T. R. Galeev, Z. A. Piazza, A. I. Boldyrev, L. S. Wang, *J. Am. Chem. Soc.* **2012**, *134*, 165; e) T. R. Galeev, C. Romanescu, W. L. Li, L. S. Wang, A. I. Boldyrev, *Angew. Chem. Int. Ed.* **2012**, *51*, 2101; *Angew. Chem.* **2012**, *124*, 2143; f) W. L. Li, C. Romanescu, Z. A. Piazza, L. S. Wang, *Phys. Chem. Chem. Phys.* **2012**, *14*, 13663; g) C. Romanescu, T. R. Galeev, A. P. Sergeeva, W. L. Li, L. S. Wang, A. I. Boldyrev, *J. Organomet. Chem.* **2012**, *721 – 722*, 148; h) L. Xie, W. L. Li, C. Romanescu, X. Huang, L. S. Wang, *J. Chem. Phys.* **2013**, *138*, 034308; i) C. Romanescu, T. R. Galeev, W. L. Li, A. I. Boldyrev, L. S. Wang, *Acc. Chem. Res.* **2013**, *46*, 350; j) Q. Chen, H. J. Zhai, S. D. Li, L. S. Wang, *J. Chem. Phys.* **2013**, *138*, 084306; k) C. Romanescu, T. R. Galeev, W. L. Li, A. I. Boldyrev, L. S. Wang, *J. Chem. Phys.* **2013**, *138*, 134315; l) H. Bai, H. J. Zhai, S. D. Li, L. S. Wang, *Phys. Chem. Chem. Phys.* **2013**, *15*, 9646; m) Q. Chen, H. Bai, H. J. Zhai, S. D. Li, L. S. Wang, *J. Chem. Phys.* **2013**, *139*, 044308; n) W. L. Li, A. S. Ivanov, J. Federič, C. Romanescu, I. Černušák, A. I. Boldyrev, L. S. Wang, *J. Chem. Phys.* **2013**, *139*, 104312; o) W. L. Li, L. Xie, T. Jian, C. Romanescu, X. Huang, L. S. Wang, *Angew. Chem. Int. Ed.* **2014**, *53*, 1288; *Angew. Chem.* **2014**, *126*, 1312; p) I. A. Popov, W. L. Li, Z. A. Piazza, A. I. Boldyrev, L. S. Wang, *J. Phys. Chem. A* **2014**, *118*, 8098; q) I. A. Popov, T. Jian, G. V. Lopez, A. I. Boldyrev, L. S. Wang, *Nat. Commun.* **2015**, *6*, 8654; r) T. Jian, W. L. Li, I. A. Popov, G. V. Lopez, X. Chen, A. I. Boldyrev, J. Li, L. S. Wang, *J. Chem. Phys.* **2016**, *144*, 154310; s) A. I. Boldyrev, L. S. Wang, *Phys. Chem. Chem. Phys.* **2016**, *18*, 11589; t) W. L. Li, T. Jian, X. Chen, T. T. Chen, G. V. Lopez, J. Li, L. S. Wang, *Angew. Chem. Int. Ed.* **2016**, *55*, 7358; *Angew. Chem.* **2016**, *128*, 7484; u) T. Jian, W. L. Li, X. Chen, T. T. Chen, G. V. Lopez, J. Li, L. S. Wang, *Chem. Sci.* **2016**, *7*, 7020; v) W. L. Li, T. Jian, X. Chen, H. R. Li, T. T. Chen, X. M. Luo, S. D. Li, J. Li, L. S. Wang, *Chem. Commun.* **2017**, *53*, 1587.
[13] a) L. S. Wang, *Phys. Chem. Chem. Phys.* **2010**, *12*, 8694; b) H. J. Zhai, L. S. Wang, D. Y. Zubarev, A. I. Boldyrev, *J. Phys. Chem. A* **2006**, *110*, 1689.
[14] a) T. T. Chen, W. L. Li, T. Jian, X. Chen, J. Li, L. S. Wang, *Angew. Chem. Int. Ed.* **2017**, *56*, 6916; *Angew. Chem.* **2017**, *129*, 7020; b) P. J. Robinson, X. Zhang, T. McQueen, K. H. Bowen, A. N. Alexandrova, *J. Phys. Chem. A* **2017**, *121*, 1849.
[15] a) W. L. Li, T. T. Chen, D. H. Xing, X. Chen, J. Li, L. S. Wang, *Proc. Natl. Acad. Sci. USA* **2018**, *115*, E6972; b) T. T. Chen, W. L. Li, J. Li, L. S. Wang, *Chem. Sci.* **2019**, *10*, 2534.
[16] P. J. Robinson, G. Liu, S. Ciborowski, C. Martinez-Martinez, J. R. Chamorro, X. Zhang, T. M. McQueen, K. H. Bowen, A. N. Alexandrova, *Chem. Mater.* **2017**, *29*, 9892.
[17] X. Chen, T. T. Chen, W. L. Li, J. B. Lu, L. J. Zhao, T. Jian, H. S. Hu, L. S. Wang, J. Li, *Inorg. Chem.* **2019**, *58*, 411.
[18] I. León, Z. Yang, H. T. Liu, L. S. Wang, *Rev. Sci. Instrum.* **2014**, *85*, 083106.
[19] See the Supporting Information for experimental details, computational methods, temperature-dependent spectra, detailed peak positions and angular distributions, all low-lying isomers, and calculated vibrational frequencies.
[20] A. P. Sergeeva, B. B. Averkiev, H. J. Zhai, A. I. Boldyrev, L. S. Wang, *J. Chem. Phys.* **2011**, *134*, 224304.
[21] J. Tao, J. P. Perdew, V. N. Staroverov, G. E. Scuseria, *Phys. Rev. Lett.* **2003**, *91*, 146401.
[22] a) J. Hay, W. R. Wadt, *J. Chem. Phys.* **1985**, *82*, 270; b) P. J. Hay, W. R. Wadt, *J. Chem. Phys.* **1985**, *82*, 284; c) P. J. Hay, W. R. Wadt, *J. Chem. Phys.* **1985**, *82*, 299.
[23] T. H. Dunning, *J. Chem. Phys.* **1989**, *90*, 1007.
[24] M. J. Frisch et al., Gaussian 09, Revision A.02, Gaussian, Inc., Wallingford, CT, **2016**.
[25] D. M. Zubarev, A. I. Boldyrev, *Phys. Chem. Chem. Phys.* **2008**, *10*, 5207.
[26] a) J. P. Foster, F. Weinhold, *J. Am. Chem. Soc.* **1980**, *102*, 7211; b) A. E. Reed, R. B. Weinstock, F. Weinhold, *J. Chem. Phys.* **1985**, *83*, 735.
[27] *CRC Handbook of Chemistry and Physics*, 85th ed. (Ed.: D. R. Lide), CRC, Boca Raton, FL, **2004**, pp. 9 – 74.

Manuscript received: February 23, 2019
Accepted manuscript online: April 25, 2019
Version of record online: May 16, 2019

